Journal of Photochemistry & Photobiology, A: Chemistry 483 (2027) 117609

Contents lists available at ScienceDirect

Journal of Photochemistry & Photobiology, A: Chemistry

journal homepage: www.elsevier.com/locate/jphotochem

Triplet quantum yield determination with noncollinear double pulse fluorescence applied to a new class of cationic free-based porphyrins

Rafael de Queiroz Garcia [a,*], Leandro H. Zucolotto Cocca [a,b], Nuno M.M. Moura [c], Maria A.F. Faustino [c], Cleber Renato Mendonça [a], Leonardo De Boni [a]

[a] Instituto de Física de São Carlos, Universidade de São Paulo, Caixa Postal 369, 13560-970 São Carlos, SP, Brazil
[b] Photonics Group, Institute of Physics, Federal University of Goiás, 74001-970 Goiânia, GO, Brazil
[c] LAQV-REQUIMTE, Department of Chemistry, University of Aveiro, 3810-193 Aveiro, Portugal

ARTICLE INFO

Keywords:
Triplet quantum yield
Intersystem crossing
Double pulse fluorescence
Fluorescence depletion
Porphyrins
Nonlinear optical spectroscopy
Ultrafast laser spectroscopy
Femtosecond transient absorption

ABSTRACT

Accurate and simple determination of key photophysical parameters, such as triplet quantum yield and intersystem crossing rate, holds significant technological importance for a series of modern biological, optical, and photonics applications. Techniques such as double- or multi-pulse fluorescence (DPF or MPF) have flexible requirements on the photophysical parameters of the samples and allow for the measurement on nanosecond timescales of the triplet quantum yield. Here, we present a novel noncollinear DPF configuration that facilitates the implementation of DPF setups for ultrafast pulsed laser systems with different divergences, beam profiles and wavelengths. We develop a framework for performing DPF experiments in both collinear and noncollinear geometries using two models, which consider either a flat-top or a Gaussian beam profile and calibration samples. In both models, a novel correction procedure for imperfect spatial overlap is implemented, which is a necessity for noncollinear DPF and most of the collinear DPF setups available. We demonstrate that the noncollinear configuration produces results equivalent within 5% relative difference to the traditional collinear setups when the flat-top beam profile model is used. Furthermore, treating the beam profile as Gaussian allowed triplet quantum yield determination at 50% lower laser fluence values due to the closer proximity to the experimental conditions. The new setup was demonstrated on a new class of recently synthesized cationic porphyrins, for which no previous photophysical characterization has been made. The triplet quantum yields of the porphyrins range between (25 ± 2)% and (35 ± 3)% and the accuracy of the technique is sufficient for the application to compounds with significant (>10%) triplet quantum yields.

1. Introduction

The Double-Pulse (DPF) and Multi-Pulse (MPF) fluorescence excitation techniques are advanced methodologies used to determine the triplet quantum yield (TQY) of emissive molecules [1–4]. These techniques involve exciting the molecules with multiple laser pulses and subsequently measuring the sequential fluorescence emissions produced. The TQY determination is performed by indirectly calculating the formation of the triplet state population on a ns-timescale between the excitations. This is carried out by evaluating the accumulated quenching of the fluorescence excited by consecutive pulses, caused by the population transfer to the excited triplet states, which normally do not fluoresce. This indirect determination is possible because excited triplet states' lifetimes are usually orders of magnitude longer than fluorescence lifetimes and, therefore, decay to the ground state is negligible during the timescale of the experiment [2].

Techniques using picosecond pulse trains [1] and double/multiple pulse excitation with pulses generated outside of the laser cavity have already been demonstrated [2,4]. Compared to transient absorption-based techniques [5,6], knowledge of the absorption cross-sections of excited states in DPF/MPF is not strictly necessary to obtain the TQY [1,4]. Also, for techniques with pump-probe schemes, working with time delays on the order of ns may pose an additional limitation, sometimes requiring the abandonment of sub-ns probes and making use of flash-photolysis setups [7]. To avoid that, the pulse train *Z*-scan method is another option for characterizing long-lived excited states [8–10]. However, this approach still requires fitting multiple parameters, such as absorption cross-sections and decay rates, and does not

* Corresponding author.
E-mail address: rafael.garcia@desy.de (R. de Queiroz Garcia).

https://doi.org/10.1016/j.jphotochem.2026.117609
Received 31 January 2026; Received in revised form 10 June 2026; Accepted 9 August 2026
Available online 10 August 2026

provide an independent measurement of the TQY. There are also other emission-based techniques besides DPF/MPF. Several studies make use of chopped continuous-wave lasers at different frequency modulations [11,12] and also of Fluorescence Correlation Spectroscopy [13,14]. A relevant advantage of using DPF over these techniques is the possibility of separately measuring the effects on the nanosecond timescale. Furthermore, it requires simpler modeling and less measurement time to measure the TQY or the intersystem crossing rate. In this manner, the photophysical parameters obtained by DPF can be inputs to these other techniques that can measure μs and ms dynamics. In addition, although DPF/MPF probe the triplet states indirectly via the fluorescence, these techniques have already been demonstrated on molecules with low fluorescence quantum yields of even ~0.1% [4].

Although presenting advantages, the DPF/MPF techniques can still have some issues that limit their accuracy. The relative spot size and spatial overlap of the beams used can impact the final result of the method, which we investigate using two new correction models and a noncollinear geometry. The models either consider a flat-top or Gaussian beam profile. The former model is simpler to apply and yields equivalent results under fluorescence saturation. The noncollinear geometry is beneficial for DPF experiments because it eliminates the necessity of using dedicated optics for collinear beam combination. This also avoids energy losses caused by the beam combination, which might be a limitation for lower pulse energy systems. In addition, it makes the setup easily adaptable to be used with different central wavelengths that improve the DPF accuracy for different materials. As will be discussed further in Section 3.3, the accuracy is improved by a high degree of excitation of the sample. Therefore, tunable laser sources can in principle be tuned to different absorption bands to excite the highest degree of population to the excited state with the lowest possible fluency. In addition, with the proposed models and a noncollinear configuration, even a pulse sequence with pulses of different wavelengths could be used to optimize the DPF signal and validate the TQY for different excitation conditions. The results of the noncollinear setup are compared to the collinear setup, which was also tested with the two correction models. The full formalism for the Gaussian beam model is presented in the Supporting Information (SI). We consider the methodology presented in this work important for enhancing the utility of DPF/MPF techniques because the only prior photophysical parameter required for the determination of the TQY is the fluorescence lifetime of the molecules, which can be measured using the same setup.

To benchmark the non-collinear setup, the TQYs of two new cationic porphyrins, Por-3,4, and their corresponding precursors, Por-1,2 [15], were determined. The determination of TQY remains crucial for porphyrins and other organic compounds across various scientific, biological, and healthcare fields [15]. For example, these compounds may be employed as photosensitizers in photodynamic therapy (PDT) for the treatment of tumors [16–18] and the photodynamic inactivation (PDI) of microorganisms [19–21]. In particular, cationic porphyrins and related compounds stand out as photosensitizers for the inactivation of viruses, fungi, protozoa, Gram-negative and Gram-positive bacteria [22–25]. However, the impact of the moieties on the intrinsic properties of the molecule, such as the TQY, is not always quantified, limiting the comprehension of the photochemical behavior of these molecules in their respective applications. For example, this work shows that the difference in TQY is almost negligible between Por-3 (30 ± 3%) and its precursor Por-1 (32 ± 3%). However, it is already significant between Por-4 (25 ± 2%) and its precursor Por-2 (33 ± 3%).

2. Synthesis and Characterization of the singlet states of the porphyrin derivatives

2.1. Synthesis of porphyrin derivatives Por-1-4

The synthetic strategy to prepare the cationic porphyrin derivatives Por-3 and Por-4 (Fig. 1) required the prior preparation of the corresponding neutral precursors Por-1 and Por-2 bearing a terpyridine moiety at a beta-pyrrolic position. These neutral derivatives were obtained through a Kröhnke-type reaction, as previously reported [15,26]. This methodology involved the reaction of the easily accessible 2-

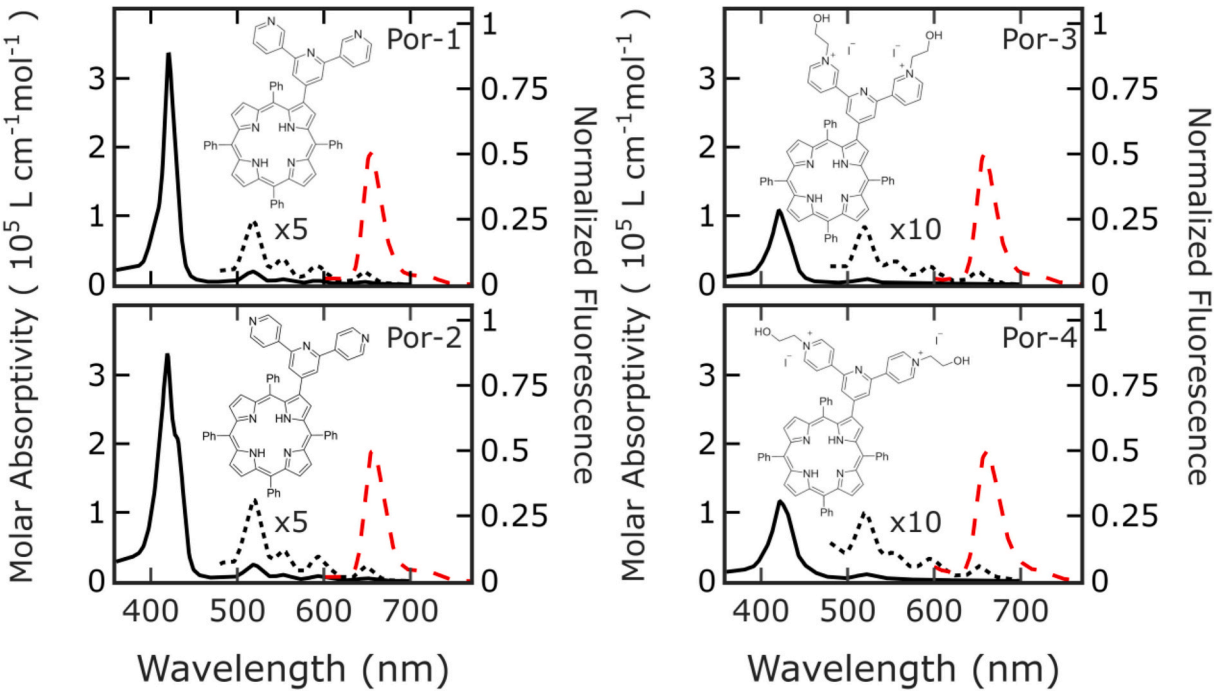

Fig. 1. Molar absorptivities (black lines) and normalized fluorescence emission spectra (red dashed lines) of the neutral (Por-1,2) and cationic (Por-3,4) porphyrin derivatives dissolved in DMSO studied here. The black dotted line represents the molar absorptivity multiplied by 5 or 10 times in the range of the Q bands. The porphyrin structure responsible for each spectrum is also included. (For interpretation of the references to colour in this figure legend, the reader is referred to the web version of this article.)

formyl-5,10,15,20-tetraphenylporphyrin with 3- or 4-acetylpyridine in the presence of ammonium acetate and catalytic amounts of $La(OTf)_3$ [15,26]. Further reaction of the appropriate neutral precursors Por-1 and Por-2 with 2-iodoethanol in refluxing chloroform afforded, after workup, the desired dicationic derivatives Por-3 and Por-4, respectively. The structures of the new compounds (Por-3 and Por-4) were unambiguously confirmed by NMR, and their molecular formulas were confirmed by HRMS (see Supporting Information, Figs. S9–S14).

2.2. Linear optical and excited singlet state measurements

In developing the new technique, it was essential to first conduct a thorough characterization of the materials involved. Therefore, the compounds were analyzed using techniques such as linear optical spectroscopy and excited-state absorption. All optical measurements were performed with porphyrins Por-1–Por-4 (Fig. 1) dissolved in dimethyl sulfoxide (DMSO). The molar absorptivities were obtained with the solutions at low concentrations ($\sim 10^{-6}$ M) employing a UV–Vis Shimadzu 1800 spectrophotometer. The results (solid lines) are shown in Fig. 1, together with the profile of the fluorescence emission spectrum (dashed red lines) acquired using a Hitachi F-7000 fluorimeter also performed in low concentration (10^{-6} mol/L) to avoid fluorescence reabsorption. The fluorescence quantum yield (φ_f) was measured using Brouwer's method [27], and using Hematoporphyrin IX in DMSO, with $\varphi_f^{ref} = 8\%$, as a reference molecule [28]. The time-resolved fluorescence, used to determine the fluorescence lifetimes of the molecules (τ_f), was measured using a setup described elsewhere [4]. The results are summarized in the Supporting Information (SI, Fig. S1).

The linear optical measurement results are shown in Table 1. The cationic porphyrins (Por-3,4) presented lower fluorescence quantum yields and fluorescence lifetimes shorter than the non-cationic ones (Por-1,2). The pyridine nitrogens in the "*para*" positions in porphyrins Por-2 and Por-4 also reduce the fluorescence quantum yield. It should be mentioned that Cocca and collaborators also observed the same pattern in meso-tetra(pyridyl)porphyrins containing peripheral polypyridyl platinum(II) complexes [10], thus confirming the accurate determination of these parameters. In addition, the lifetimes of the materials are on the order of 10 ns, and it is possible to observe that Por-3 and Por-4 exhibit lower fluorescence lifetimes than Por-1 and Por-2.

With the fluorescence lifetime and quantum efficiency determined, the compounds were further investigated to characterize their excited states. This step was essential due to the potential presence of charge transfer processes in the excited state. To facilitate this, the well-known *Z*-Scan technique and the transient absorption technique were employed. The transient absorption technique is based on exciting the molecules with a pulsed laser beam (~150 fs) at 390 nm and a 1 kHz repetition rate, while probing the response using a white light continuum pulse [29]. The results have shown that no ultrafast dynamics were observed at the magic angle; only a plateau was seen up to 10 ps after excitation (see Fig. S3). Thus, no evidence of charge transfer could be observed, not influencing the results from the proposed technique.

Through the open aperture *Z*-Scan technique, it was possible to determine the excited state absorption cross-sections of the compounds. First, the absorption cross-section at 532 nm was determined using a femtosecond laser (detailed information on the experimental procedure can be found at: [30]). Fig. S2 exhibits the experimental open aperture Z-scan technique and theoretical fitting for porphyrins Por-1—Por-4.

Table 1
The measured fluorescence quantum yields and fluorescence lifetimes for the four molecules.

	Por-1	Por-2	Por-3	Por-4
φ_f(%)	3.7	2.7	2.4	0.7
τ_f (±0.5 ns)	9.9	10.5	8.9	6.5

With the absorption cross-section at 532 nm in hand, the full spectrum of absorption cross-sections was then obtained using the transient absorption technique. The method for obtaining these results is described in the literature [31].

Fig. 2 presents the spectra of the excited-state absorption cross-sections, $S_1 \rightarrow S_n$ (σ_{1n}, red lines) and the $S_0 \rightarrow S_1$ absorption cross-sections (σ_{01}, black lines). From this figure, it can be seen that the excited-state absorption bands occur in the same spectral regions as the ground-state absorption bands ($S_0 \rightarrow S_1$). Additionally, the values of the excited-state absorption cross-sections are comparable to those of the ground state, i.e., $\sigma_{01}(\lambda) \sim \sigma_{1n}(\lambda)$. Comparison of these values with those reported in the literature for similar compounds reveals considerable agreement. For example, Cocca et al. reported a σ_{1n} (532 nm) between 1.9 and 3.1 $\times 10^{-17}$ cm^2 for phthalocyanine derivatives [32], and σ_{1n} (532 nm) around 1.3 $\times 10^{-17}$ cm^2 and 2.0 $\times 10^{-17}$ cm^2 for tetracarboxy Zn and Al phthalocyanines derivatives [19]. Regarding the class of porphyrins, studies have reported excited-state absorption cross-sections ranging from 1.4 $\times 10^{-17}$ cm^2 and 4.5 $\times 10^{-17}$ cm^2 for isomeric meso-tetra(pyridyl)porphyrins containing peripheral polypyridyl platinum(II) complexes [10]. In addition, Gotardo et al. determined a cross-section of approximately 1.75 $\times 10^{-17}$ cm^2 at 532 nm for Protoporphyrin IX [9]. It should be highlighted that all the mentioned studies utilized the *Z*-scan technique with white light pulses [33] for the $\sigma_{1n}(\lambda)$ determination. Based on this comparison, there is strong agreement between the excited-state absorption cross-section values obtained in this work and those reported in the literature, indicating that these parameters have been accurately determined.

All of these measurements provide a broad characterization of the singlet states of the four porphyrins (Por-1-Por-4), also revealing that there is excited state absorption at 515 nm, with similar ground and excited state cross-sections. It should be mentioned that this is the wavelength that will be used in the DPF experiment. Thus, this result assures that the first excited singlet state can be almost fully populated when optical saturation is reached and when the ultrafast relaxation of higher excited states to the S_1 has taken place, after the end of the excitation.

With these key spectroscopic parameters of the materials now determined, we can proceed to apply the proposed techniques.

3. Characterization of the triplet states

3.1. Theory of double-pulse fluorescence experiments

The DPF experiment works by using two sub-ns pulses of similar energy, delayed by a time ΔT and focused on the same sample spot. As depicted in Fig. 3(a), the double excitation induces a fluorescence decay. By time-resolving the fluorescence decay using a fast detector, it is possible to fit its amplitude as a function of time. This is done by convoluting two consecutive exponentials with the instrument response function and using the sample's fluorescence lifetime as input. In the Supporting Information, one can find more details about the fitting model, which is the same as in previous work [4]. The time-dependent fluorescence amplitude is associated with the first excited state population ($N_{S_1}(t)$) by a detection efficiency constant (α). Hence, a model for indirectly determining the TQY (φ_T) using the first excited state population can be introduced. This model will be responsible for associating the amount of quenching in the fluorescence with the triplet state population.

For the modeling, two distinct time scales must be considered. Whereas excitation is performed with ultrashort pulses (< 10 ps), fluorescence emission and intersystem crossing dynamics happen on the nanosecond time scale. So, the correct assumptions need to be made to avoid unnecessary complications in data analysis. Therefore, here we propose the use of a simplified three-state system for modeling the DPF experiments on the ns time scale [1,4]. These states consist of the ground singlet state (S_0), lower excited state (S_1), and lower excited triplet state

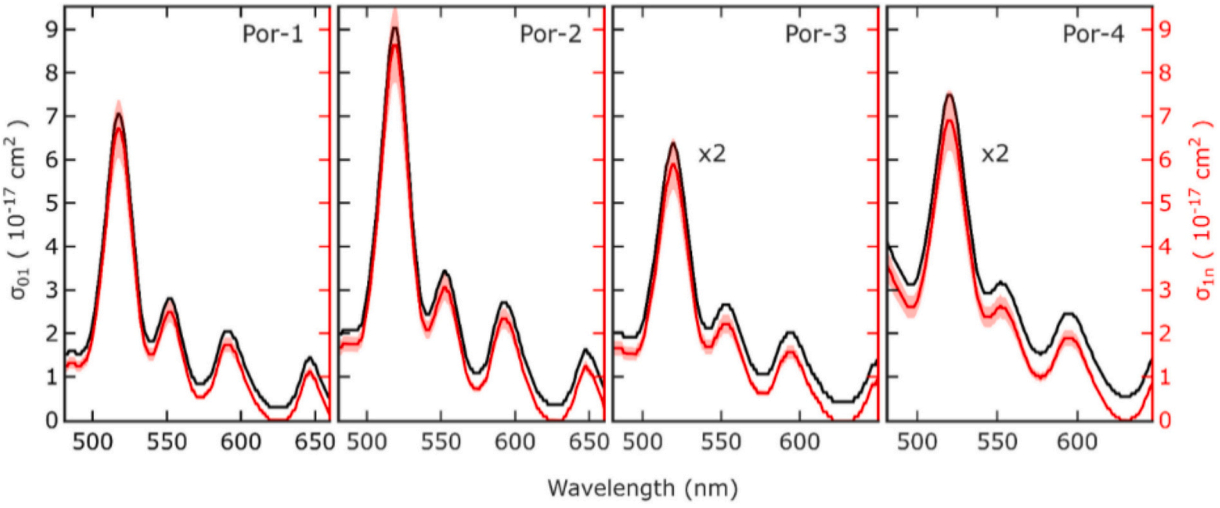

Fig. 2. Excited state absorption cross-sections (σ_{1n}, red lines) obtained with transient absorption spectroscopy for Por-1—Por-4. They are compared with the $S_0 \rightarrow S_1$ absorption cross-sections (σ_{01}, black lines). For Por-3 and Por-4, the values of both cross-sections were multiplied by two to match the same scale as Por-1 and Por-2. The error in the determination of σ_{1n} is reported as a continuous red band. (For interpretation of the references to colour in this figure legend, the reader is referred to the web version of this article.)

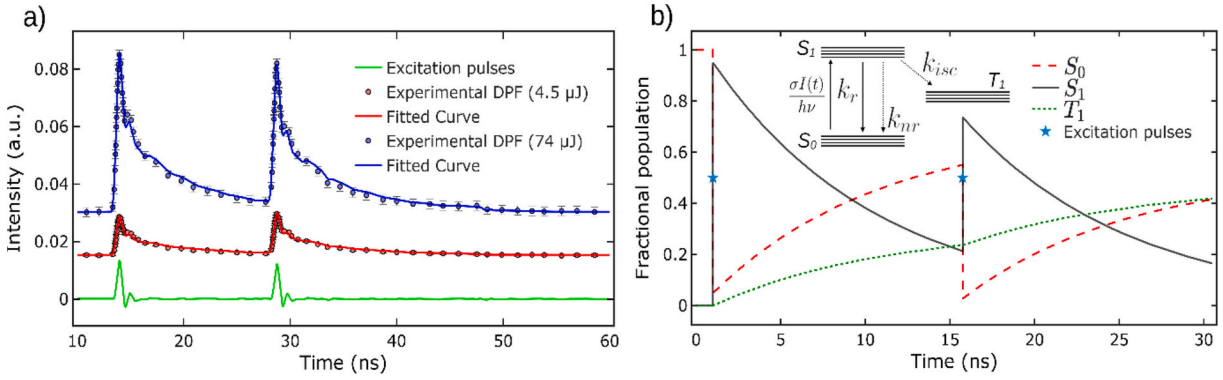

Fig. 3. a) Typical DPF measurements are shown for different excitation pulse energies (pulses with 4.5 μJ and 74 μJ). The green curve shows the energy amplitude of each DPF pulse and the temporal response of the detector. By using eq. SI1 in SI, it is possible to fit the DPF data for each pulse energy (blue and red curves). b) A theoretical model with three energy states (S_0, S_1, and T_1) is simulated in a DPF experiment with pulses spaced from $\Delta T = 14.75\ ns$ and energies that excite ~95% of the molecules in the ground state. The k_r,k_{nr}, and k_{isc} are the radiative, non-radiative, and intersystem crossing rates. (For interpretation of the references to colour in this figure legend, the reader is referred to the web version of this article.)

(T_1). In this framework, k_r, k_{nr}, and k_{isc} are the rates for the radiative, non-radiative, and intersystem crossing processes. The fluorescence lifetime is given by $\tau_f = \frac{1}{k_r + k_{nr} + k_{isc}}$ and these quantities are related to the fluorescence, triplet and internal conversion quantum yields by $\varphi_F = k_r\tau_f$, $\varphi_T = k_{isc}\tau_f$ and $\varphi_{IC} = k_{nr}\tau_f$, respectively. This three-state model adequately describes several organic systems, like porphyrins and phthalocyanines [9]. The reason for eliminating the use of other excited states is that any optical excitation to other higher singlet states during the time of the pulse will result in ultrafast internal conversion and relaxation to the bottom of S_1, which will typically have a ns lifetime. Such ultrafast relaxation deactivates the stimulated emission channel upon optical excitation far from the emission wavelengths of the molecule. Also, by doing so, it allows for a laser beam to optically saturate a region of the sample by almost completely depopulating S_0. This is the desired effect for maximizing the population transferred to the triplet state after excitation by one pulse and will be a central assumption in the modeling. If, however, the emission and absorption spectra overlap at the excitation wavelength, full population inversion will not be achieved, and this must be considered in the analysis of the TQY. Yet, even for laser dyes, such as rhodamine 6G, it is possible to select an excitation wavelength under which not only this stimulated emission fluorescence quenching effect is avoided [34], but the molecule even presents excited state absorption [35].

Now, a derivation for obtaining φ_T will be outlined. One starts by writing the rate equations (Eq. (1) to (3)) corresponding to the three states of the model in Fig. 3b).

$$\frac{dN_{S_0}}{dt} = -N_{S_0}\frac{\sigma_{01}}{h\nu} I_p(t) + \frac{N_{S_1}}{\tau_f}(1-\varphi_T); \tag{1}$$

$$\frac{dN_{S_1}}{dt} = +N_{S_0}\frac{\sigma_{01}}{h\nu} I_p(t) - \frac{N_{S_1}}{\tau_f}; \tag{2}$$

$$\frac{dN_{T_1}}{dt} = \varphi_T\frac{N_{S_1}}{\tau_f}. \tag{3}$$

In the last equations, $I_p(t)$ is the time-dependent intensity of the excitation pulse p, and N_{S_0,S_1,T_1} are the populations of each of the three states. The central photon energy of the excitation pulse is $h\nu$, and σ_{01} is the absorption cross-section at the same wavelength. Now, defining $F_p = \int_{-\infty}^{+\infty} I_p(t)dt$ and the population transfer parameter $\delta_p = \left(1 - \exp\left(-\frac{\sigma_{01}}{h\nu}F_p\right)\right)$, the rate equations (Eq. (1)–(3)) can be solved step-

wise. First, during the ultrafast excitation, no relaxation from the S_1 state occurs to either the T_1 or S_0 state. Afterwards, the slow ns relaxation is applied as in Eqs. (1) to (3) [1,3], yielding the following populations for a time t after the excitation pulse:

$$N^p_{S_0}(t) = N_{S_0}(0_-)(1-\delta_p) + N_{S_0}(0_-)\,\delta_p\left(1-\exp\left(-\frac{t}{\tau_f}\right)\right)(1-\varphi_T); \quad (4)$$

$$N^p_{S_1}(t) = N_{S_0}(0_-)\,\delta_p \exp\left(-\frac{t}{\tau_f}\right); \quad (5)$$

$$N^p_{T_1}(t) = N_{S_0}(0_-)\varphi_T\delta_p\left(1-\exp\left(-\frac{t}{\tau_f}\right)\right). \quad (6)$$

The superscript p of the populations is introduced to refer to the excitation pulse. $N_{S_0}(0_-)$ is the total number of molecules in S_0 at time $t = 0_-$. The subscript "$-$" indicates the time right before the excitation takes place. Furthermore, one should note that the fluorescence intensity, proportional to $N^p_{S_1}(t)$, is dependent on $N_{S_0}(0_-)$, δ_p, and τ_F. Thus, with the fluorescence induced for any of the two pulses alone ($N^1_{S_1}(t)$ and $N^2_{S_1}(t)$), it is not possible to obtain φ_T. However, with excitation by pulse 2 at a time ΔT after pulse 1, like in Fig. 3, the fluorescence immediately after excitation, named $N^{1\to2}_{S_1}(t=\Delta T)$ ($t = \Delta T + \tau_{pulse} \sim \Delta T$), will be:

$$N^{1\to2}_{S_1}(\Delta T) = N^1_{S_1}(\Delta T) + \delta_2\, N^1_{S_0}(\Delta T) \quad (7)$$

By assuming that $N_{S_0}(0_-)$ can be different for each pulse ($N^p_{S_0}(0_-)$), and that $\Delta n = \frac{N^2_{S_0}(0_-) - N^1_{S_0}(0_-)}{N^1_{S_0}(0_-)}$, one can write a more general expression for $N^{1\to2}_{S_1}(\Delta T)$:

$$N^{1\to2}_{S_1}(\Delta T) = N^1_{S_1}(\Delta T) + \delta_2\left(N^1_{S_0}(\Delta T) + N^1_{S_0}(0_-)\Delta n\right) \quad (8)$$

Physically, the Δn parameter means that the second pulse induces fluorescence in a different population than the first one, which must be accounted when calculating the TQY. For instance, if $\Delta n > 0$, the second pulse induces fluorescence in a population that was not excited by the first pulse. This means that no molecules in this new Δn population are in the triplet state, and the quenching of the fluorescence will be smaller than expected, but the TQY must stay the same for any Δn value. Now, it is important to define the relative fluorescence amplitude (r_{fluor}), given by $r_{fluor} = \frac{N^{1\to2}_{S_1}(\Delta T)}{N^1_{S_1}(0)}$, which is a quantity accessible experimentally by the time-resolved fluorescence measurements (Eq. SI1 in SI). With these considerations, one can solve for φ_T in Eq. 8 [2]:

$$\varphi_T = 1 - \frac{\left(r_{fluor} - \exp(-\Delta T/\tau_f)\right)\delta_1 + (\delta_1 - 1 - \Delta n)\,\delta_2}{\delta_1\,\delta_2\left(1-\exp(-\Delta T/\tau_f)\right)} \quad (9)$$

Thus, the problem of determining φ_T is reduced to the problem of determining r_{fluor}, Δn, and δ_p. In optical saturation, when $\delta_1, \delta_2 \to 1$, the result is simply $\varphi_T = \frac{1 - r_{fluor} + \Delta n}{1-\exp(-\Delta T/\tau_f)}$, which makes φ_T independent of δ_p. This shows why it is useful to reach optical saturation in DPF/MPF-like experiments. It eliminates the necessity of knowing the populations in the excited states. However, the modeling as described here, which will hereafter be called **model 1**, only works at optical saturation. One factor that may change the fluorescence before achieving the saturation is the spatial dependence of the laser beam profile, which can be better approximated by a Gaussian instead of the effective flat-top description of **model 1**. The introduction of a Gaussian beam profile will be called **model 2**. This kind of improvement in the model has, to the best of our knowledge, not yet been done in DPF experiments that used population transfer curves of the form $\delta_p(r) = \left(1-\exp\left(-\frac{\sigma_{01}}{h\nu}F_p(r)\right)\right)$ [1,4]. Hence, the formalism for this change is developed in the SI for the case of collinear pulses with equal or different beam waists, thus accounting for the fact that each pulse may have a different effective focal volume.

3.2. Noncollinear DPF

The DPF setup, depicted in Fig. 4, was performed with the second harmonic of a Pharos laser system (Light Conversion), which provides 220 fs laser pulses centered at 515 nm. This output was stretched to approximately 1.5 ps and was set to work at a low repetition rate < 10 Hz in all the measurements to avoid distinct cumulative thermal lens dynamics under single and double pulse operations. The noncollinear configuration requires only one beam splitter to create two beams. A broadband beam splitter can be used in the case of a tunable source. One beam is sent to a delay line of $\Delta T = 15.45\,ns$, and both beams are aligned to spatially overlap at the sample, being focused by the same f = 250 mm lens. The sample is placed in a 2 mm length cuvette and the absorbance is set to 0.2 at 515 nm by choosing the correct concentration. All the measurements are done at ambient temperature (25 °C). The fluorescence is collected at positions where the beam waist w ranges between 200 and 400 μm. This is done using an optical cable with a 1 mm core diameter. The cable then directs the light to a fast silicon photodetector, with a response time of circa 0.7 ns (Fig. 3 a), green curve). A digital 1 GHz bandwidth oscilloscope is used to acquire the data. All the samples using of the same calibration sample are measured keeping the same position relative to the optical cable and the same beam alignment.

The measurements in this work are performed with double pulses with very similar energies, with the energy ratio 1.0 ± 0.1, and the common attenuation of both pulses is done directly at the laser output. The fluorescence intensity is measured as a function of pump pulse energy to construct the fluorescence curves ($N^1_{S_1}, N^2_{S_1}$, and $N^{1\to2}_{S_1}$). This allows one to obtain the excited state population transfer as a function of laser power (δ_1, δ_2), which is necessary for obtaining the correct triplet values mainly at lower fluencies. In the case of noncollinear DPF, two measurements are performed for each pulse energy. First, the second fluorescence is recorded by blocking the first pulse with a beam block. This allows the measurement of $N^2_{S_1}$. Then, with both pulses unblocked, the first fluorescence $N^1_{S_1}$ and the sequential fluorescence $N^{1\to2}_{S_1}$ can be recorded from the time resolved signal as in Fig. 3 a).

Previous work in the literature already pointed out the use of collinear DPF with a double-pulse train created by a beam splitter and an additional beam combiner [2]. Here, however, the noncollinear setup eliminates the necessity of the beam combiner. A further improvement relative to previous DPF setups is the use of an optical telescope in the delay line. With this addition, are able to deal with the slightly diverging beam and optimize for optimal mode overlap with the first beam in the sample. This is necessary since the second beam increases its size during the propagation in the delay line. Furthermore, we demonstrate how, even with a crossing angle of ~5° in the noncollinear geometry, it is possible to obtain the φ_T value when working close to the saturated fluorescence regime by measuring the fluorescence of the second pulse independently and then the DPF sequence. It is important to note that the independent characterization of the second pulse's fluorescence is not possible for lasers that already have a double pulse train (Fig. 4 b)). Additionally, working with an optical cable instead of a lens is advantageous for having less contribution from the fluorescence produced by the off-axis portion of the laser beams. Because of the lower off-axis laser intensity, the average off-axis population transferred to the triplet state is lower, and the fluorescence depletion is not as high. With **model 2**, presented in the SI, one can model this by an effective integration radius for the Gaussian beam, which is collimated by the optical cable. Also, different from FCS experiments [14], this technique can be performed on a single-shot basis for each desired laser power under low repetition rates (e.g. < 10 Hz), allowing one to obtain and analyze the results within minutes.

3.2.1. Analysis of noncollinear DPF (*model 1*)

The procedure used in this work was to perform measurements of the

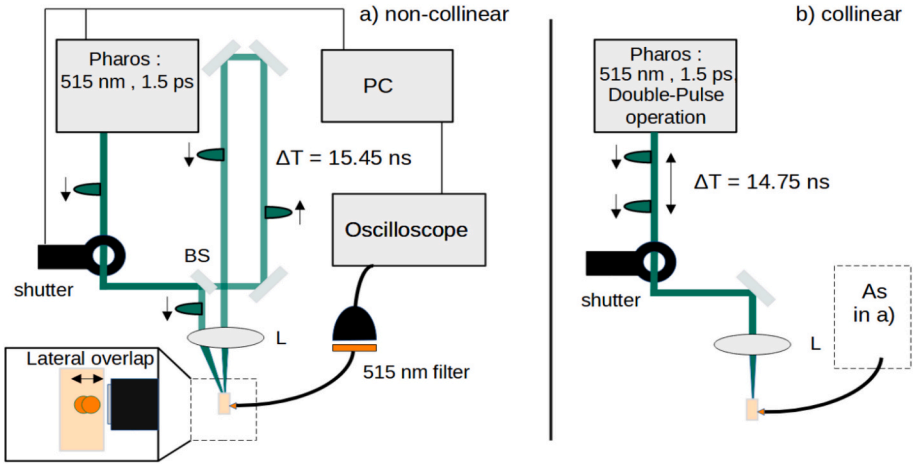

Fig. 4. The experimental scheme for the noncollinear DPF setup (a), which uses a beam splitter (BS) and a f = 250 mm convergent lens (L) for focusing the double pulse. The overlap at the sample is achieved by keeping the second beam aligned on a straight line and moving the first beam, moving the BS slightly. Due to the longer path of the delayed beam, its size can be adjusted with a two-lens telescope, not shown in the picture. For comparison, the setup for collinear DPF using double pulse operation of a cavity is also shown (b).

fluorescence intensity as a function of laser pulse energy (fluorescence curves $N^1_{S_1}, N^2_{S_1}$, and $N^{1\to2}_{S_1}$). With this, it is possible to first determine $r_{fluor} = \frac{N^{1\to2}_{S_1}(\Delta T)}{N^1_{S_1}(0)}$ by the time-resolved fluorescence measurements (see Fig. 3a)). Then, one should use the formalism of DPF to determine the population transfer to the excited state (δ_p) for any pulse energy, not only on optical saturation. This is done by fitting the $\frac{\sigma_{01}}{h\nu}$, $N_{S_0}(0_-)$ and Δn parameters of the fluorescence curves via a Non-linear Least Squares algorithm. The sample is considered to be in the saturated regime when δ_1, $\delta_2 > 0.9$ (90% population inversion). For each different beam waist size and for a specific position of the collection optics, $N_{S_0}(0_-)$ and Δn may present different values, because they describe the effective coupling of the fluorescence induced by each pulse with the optical fiber. In the noncollinear DPF setup, one uses the $N^1_{S_1}, N^2_{S_1}$ curves to obtain Δn. For each sample position, a global fitting procedure for Δn was performed, including the samples of interest and the samples of calibration. This creates self-consistency in the measurements because Δn should be constant if there are no changes in the optical components or alignment. In these fittings, $\frac{\sigma_{01}}{h\nu}$ is left as a free parameter that represents an effective absorption cross-section for the excitation.

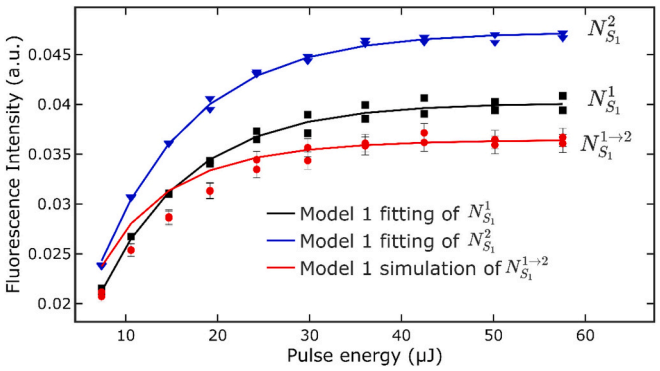

Fig. 5. The figure shows the use of **model 1** to fit the noncollinear experiment results of the Por-2 sample. One can fit the saturation of the fluorescence of the first (black squares) and second (blue triangles) pulses alone ($N^1_{S_1}$ and $N^2_{S_1}$, respectively). Then, with the obtained quantum yield from Fig. 6, one can simulate the experimental sequential fluorescence $N^{1\to2}_{S_1}$ values (red dots) with the red line. (For interpretation of the references to colour in this figure legend, the reader is referred to the web version of this article.)

3.3. Experimental results

3.3.1. Noncollinear DPF

The noncollinear DPF experiment was performed for the 4 porphyrins (Por-1—Por-4) and also with rhodamine B in DMSO and rhodamine 6G in ethanol. The rhodamines were used as calibration samples with insignificant TQY ($\varphi_T < 0.1\%$) [35,36]. The measurements were done for three different sample positions with respect to the lens focal point (See Supporting Information Table S1), which required different collimations of the second pulse relative to the first pulse. This procedure provided two beams with similar w values. The difference between the first fluorescence curve ($N^1_{S_1}$) and the second ($N^2_{S_1}$) at optical saturation was not allowed to be higher than 40% in any measurement. This assured, together with a visual inspection, that the w values were not so distinct. Then, the results were analyzed using **model 1**. A result for Por-2 is shown in Fig. 5. One can see that $N^2_{S_1} > N^1_{S_1}$, so the Δn correction must be introduced to calculate the TQY properly. With all the parameters obtained from fitting $N^1_{S_1}$ and $N^2_{S_1}$ (see Fig. 5), the TQY can be obtained as a function of the pulse energy used (Fig. 6).

As expected, the result at fluorescence saturation, at pulse energies above 30 μJ, is constant. The average value in this region should then be considered the correct value of φ_T. The incorrect values of φ_T at lower energies are caused by the inability of **model 1** to describe the real values of $N^{1\to2}_{S_1}$ in this region using only the $N^2_{S_1}$ curve. If one uses the obtained φ_T to simulate the expected $N^{1\to2}_{S_1}$ curve (Fig. 5, blue line), it is possible to see that the experimental points are only well described in the same region in which φ_T is constant in Fig. 6. This result is general for collinear and noncollinear DPF analyzed by **model 1**. The experimental error bars, associated mainly with a 10% error in the fluorescence intensities measured, do not explain the uncertainty for low energy values. Hence, **model 1**, unless improved, can only be used when optical saturation can be achieved, i.e., the population profile becomes closer to a flat-top profile in the central region of the beam. The results of using this model for all the samples with noncollinear DPF are shown in Table 2. One can note that the results match the ones obtained by collinear DPF within 5% relative difference in the φ_T value. Thus, the factor of using different w values also did not affect the analysis using **model 1**. This means that the noncollinear experiment, with its versatility of being adaptable to any short-pulsed laser system easily, can be used for measuring the TQY of organic molecules in solution with the proposed methodology.

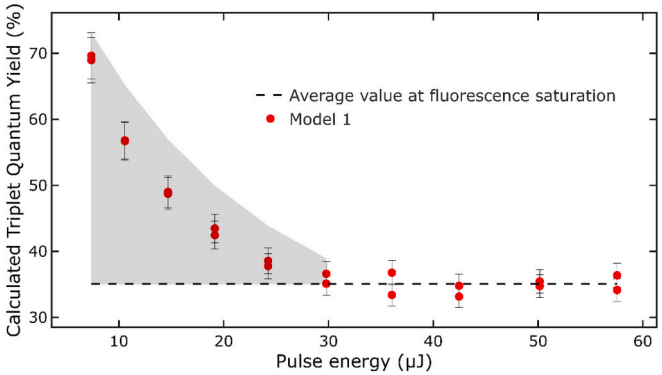

Fig. 6. Considering the fluorescence curves from Fig. 5, one is able to calculate the TQY of molecule Por-2. The shaded area shows the values for which optical saturation has still not been reached.

Table 2
The noncollinear and collinear experiments were repeated for each one of the samples in DMSO for three different beam size values. The averaged results are shown for the noncollinear experiment fitted with **model 1** and the collinear experiment fitted with **models 1** and **2**, respectively. The values are separated by semicolons. The errors for the measurements are estimated to be within 10% of the reported value. The φ_{IC} values were truncated to the second significant figure.

	φ_T (%)			
Porphyrin	Por-1	Por-2	Por-3	Por-4
Noncollinear (model 1)	32	33	30	25
Collinear (models 1; 2)	32; 33	34; 35	31; 32	26; 26
	φ_{IC} (%)			
Calculated by model 1	64	64	68	74

3.3.2. Collinear DPF

The same samples were used in this experiment. Three different beam waist values were used in the analysis to assure the modeling was reproducible for different experimental conditions. Different from the noncollinear DPF, this experiment will be used to compare the 2 models that were proposed. The Δn values, in this case, are much smaller, being less than 10% of the $N_{S_1}^1$ value at saturation when **model 1** is applied. This is a consequence of using collinear pulses with approximately equal waists. A typical result of this experiment is shown in Fig. 7.

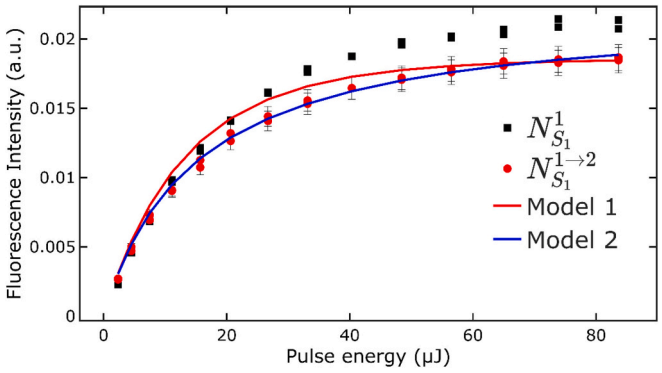

Fig. 7. A collinear DPF measurement for Por-4 is shown. Using the pulse parameters obtained from fitting a collinear experiment with Rhodamine 6G in ethanol and Rhodamine B in DMSO, one is able to simulate $N_{S_1}^{1\to2}$ (red dots) for Por-4 after fitting the $N_{S_1}^1$ curve (black squares). For this to be done, the result of the obtained TQY (Fig. 8) is used. One sees that using **model 2** considerably improves the description of the fluorescence curve.

The successfulness of the modeling depends on how the parameters obtained by the calibration sample allow the description of the $N_{S_1}^{1\to2}$ experimental points for an arbitrary sample. One sees in Fig. 7 that a considerable improvement can be observed for **model 2**, and this improvement is also reflected in the φ_T determination, as depicted in Fig. 8. With **model 2**, a more refined description of the population at the excited state is achieved, and this allows one to obtain the values of φ_T for pulse energies below the saturation energy ($>$ 40 μJ in Fig. 8). For example, at 26 μJ, the results already converge. For the beam waist of 257 μm used in the measurement of Fig. 8, this means a $\sim$ 50% reduction of the necessary peak fluence, from 0.046 J/cm^2 (48 μJ) to 0.025 J/cm^2 (26 μJ).

3.4. Discussion

Comparing the φ_T values obtained in the saturated regime by the two models (Table 2), one notices that **model 2** predicts values on average 3% higher in relative terms for φ_T. This difference is, however, smaller than the experimental error, on the order of $\pm 0.1\varphi_T$. In this way, effectively, **model 1** is adequate for describing the TQY at optical saturation. If the sample is too sensitive to photodamage, the spatially dependent formalism still needs to be used to obtain the correct values at lower fluencies. In the case of Por-3, the lower absorption cross-section was almost limiting to obtain precise TQY values because of the onset of nonlinear effects on the solvent (see Supporting Information). An alternative to reach optical saturation more easily would be to excite the band at 410–420 nm, which has an order of magnitude higher absorption cross-section (Fig. 1). This would be possible to implement combining our noncollinear setup with a tunable source pumped by our laser system, e.g., an optical parametric amplifier. Because of the lower pulse energies that would be available with such a source, this implementation would benefit from the noncollinear configuration because of the reduced losses. Furthermore, fluorescence polarization anisotropy dependence was also adapted to **model 2** [37] and the equations with these considerations are developed in the SI. However, negligible differences were observed in the regime of intensities used.

Now, comparing the results for Por-1–Por-4, the change in TQY of Por-3 relative to Por-1 is minimal, as also happened with the other photophysical quantities. However, for Por-4, one sees the decrease in φ_f relative to Por-2 is also followed by a decrease in φ_T. Thus, it becomes clear that the internal conversion pathway (assuming $\varphi_{IC} = 1 - \varphi_T - \varphi_f$), with nonradiative relaxation, is slightly favored by the cationic modification. The φ_{IC} values were calculated in Table 2 using the results for φ_f in Table 1. This decrease of the TQY value is not necessarily a factor that decreases the potential of the molecule for PDT/PDI because it is not an order of magnitude change. As has already been shown for

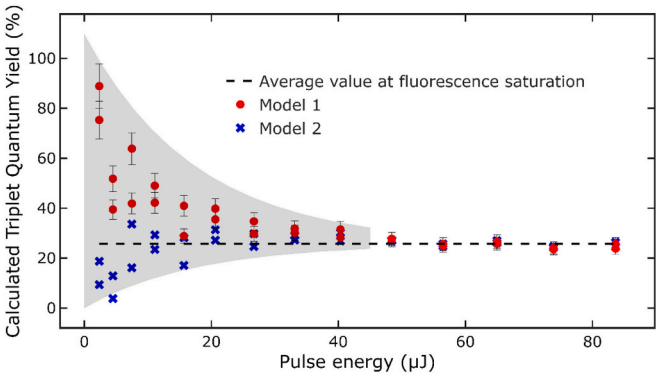

Fig. 8. The calculated TQY values for the Por-4 sample as a function of pulse energy are shown to stabilize as the fluorescence saturates. The gray region shows the values before 90% of the population is excited from S_0 to the S_1 state by each pulse.

other cationic derivatives of Por-1,2 [15], the *para*-substituted methylated derivative had higher singlet oxygen efficiencies than the *meta*-substituted isomer. The *para* isomer also had a performance comparable to the cationic 5,10,15,20-tetrakis(1methylpyridinium-4-yl)porphyrin. Hence, the main factor that seemed to influence the singlet oxygen production was the charge distribution of the molecule and the proximity of the iodine anion to the positive charge of the pyridinium cations [15].

Concerning the order of magnitude of φ_T values obtained, they are in accordance with the previous reported results regarding similar compounds. One can use, e.g., meso-tetra-(pyridyl)porphyrins dissolved in DMSO as a base for comparison. Previous works have measured the effect of the Nitrogen position in the pyridine ring on φ_T and other photophysical parameters [4,10]. A study containing peripheral polypyridyl platinum(II) complexes showed that the *para*-Pt(II) substituted porphyrin ($\varphi_T = 12\%$) exhibited a decrease of φ_T relative to the *meta*-Pt (II) substituted ($\varphi_T = 44\%$) and the *meta* free base tetra(pyridyl) porphyrin ($\varphi_T = 39\%$) [10]. As in the current case between Por-3 and Por-4, this was caused by a considerable increase of the nonradiative relaxation of the *para*-isomer. In the case of another study with cationic meso-tetra(cisplatin)porphyrins [4], φ_T ranged between 48 and 50% for both isomers dissolved in DMSO, without a considerable relative increase of the nonradiative rate for the *para* isomer.

4. Conclusion

This article proposed a new methodology both for the collinear and noncollinear DPF techniques, also showing the comparison of two models valid for different fluence regimes of the excitation pulses. Noncollinear DPF is useful for easily adapting any ultrashort-pulsed laser to perform a DPF experiment. The setup that can be used with a tunable source and possibly, in the future, even with a pulse sequence with pulses of different central wavelengths. Furthermore, the linear and excited state photophysical characterization of the two neutral and two new cationic porphyrin derivatives was carried out. Values of TQY between 25% and 35% were measured and by the typical intensity noise of 10% the technique is expected to work accurately for molecules with significant TQY values, above 10%. With noncollinear DPF, it was shown that the relative increase in the nonradiative internal conversion pathway is different for each cationic porphyrin relative to its non-cationic form and that the technique is sensitive to these changes. Finally, it should be highlighted that the photophysical parameters determined in this work are in agreement with results previously reported in the literature for cationic and non-cationic meso-tetra-(pyridyl)porphyrins. This demonstrates the effectiveness of the technique for determining the triplet quantum yield of materials for future applications in optics and photonics.

CRediT authorship contribution statement

Rafael de Queiroz Garcia: Writing – original draft, Validation, Methodology, Investigation. **Leandro H. Zucolotto Cocca:** Writing – review & editing, Visualization, Validation, Methodology, Investigation. **Nuno M.M. Moura:** Writing – review & editing, Resources, Investigation, Conceptualization. **Maria A.F. Faustino:** Writing – review & editing, Resources, Investigation, Conceptualization. **Cleber Renato Mendonça:** Writing – review & editing, Funding acquisition. **Leonardo De Boni:** Writing – review & editing, Visualization, Validation, Supervision, Resources, Methodology, Investigation, Funding acquisition, Conceptualization.

Declaration of competing interest

The authors declare that they have no known competing financial interests or personal relationships that could have appeared to influence the work reported in this paper.

Acknowledgments

Thanks are due to the University of Aveiro, FCT/MCT for the financial support for the LAQV-REQUIMTE (UIDB/50006/2020) and the FCT project PORP2PS (EXPL/QUI-QOR/0586/2021), through national funds and, where applicable, co-financed by the FEDER, within the PT2020 Partnership Agreement. N.M.M. Moura thanks his research contract CDL-CTTRI-048-88-ARH/2018 which is funded by national funds (OE), through FCT, in the scope of the framework contract foreseen in the numbers 4, 5 and 6 of the article 23, of the Decree-Law 57/2016, of August 29, of August 29, changed by Law 57/2017, of July 19. Thanks are also due to Prof. M. Graça P. M. S. Neves of University of Aveiro for helpful chemical discussions. Financial support from FAPESP (Fundação de Amparo à Pesquisa do Estado de São Paulo, grants 2016/20886-1, 2018/11283-7 2020/16036-8, 2020/15966-1 and 2022/02439-9), CNPq (Conselho Nacional de Desenvolvimento Científico e Tecnológico, Coordenação de Aperfeiçoamento de Pessoal de Nível Superior (CAPES) Finance Code 001, Army Research Laboratory (W911NF-17-1-0123) and Air Force Office of Scientific Research (FA9550-12-1-0028) are acknowledged.

Appendix A. Supplementary data

Supplementary data to this article can be found online at https://doi.org/10.1016/j.jphotochem.2026.117609.

Data availability

Data will be made available on request.

References

[1] L. De Boni, P.L. Franzen, P.J. Gonçalves, I.E. Borissevitch, L. Misoguti, C. R. Mendonça, S.C. Zilio, Pulse train fluorescence technique for measuring triplet state dynamics, Opt. Express 19 (2011) 10813, https://doi.org/10.1364/OE.19.010813.

[2] S. Reindl, A. Penzkofer, Triplet quantum yield determination by picosecond laser double-pulse fluorescence excitation, Chem. Phys. 213 (1996) 429–438, https://doi.org/10.1016/S0301-0104(96)00289-3.

[3] S.D.M. Islam, A. Penzkofer, P. Hegemann, Quantum yield of triplet formation of riboflavin in aqueous solution and of flavin mononucleotide bound to the LOV1 domain of Phot1 from Chlamydomonas reinhardtii, Chem. Phys. 291 (2003) 97–114, https://doi.org/10.1016/S0301-0104(03)00187-3.

[4] D.C. Jornada, Rafael de Queiroz Garcia, C.H. da Silveira, L. Misoguti, C. R. Mendonça, R.C.V. Santos, L. De Boni, B.A. Iglesias, Investigation of the triplet excited state and application of cationic meso-tetra(cisplatin)porphyrins in antimicrobial photodynamic therapy, Photodiagn. Photodyn. Ther. 35 (2021) 102459, https://doi.org/10.1016/j.pdpdt.2021.102459.

[5] D. Peceli, S. Webster, D.A. Fishman, C.M. Cirloganu, H. Hu, O.V. Przhonska, V. V. Kurdyukov, Y.L. Slominsky, A.I. Tolmachev, A.D. Kachkovski, R.R. Dasari, S. Barlow, S.R. Marder, D.J. Hagan, E.W. Van Stryland, Optimization of the double pump–probe technique: decoupling the triplet yield and cross section, J. Phys. Chem. A 116 (2012) 4833–4841, https://doi.org/10.1021/jp301051u.

[6] S. Reindl, A. Penzkofer, H. Gratz, Intersystem-crossing and excited-state absorption of C70 studied by picosecond pump and probe absorption and fluorescence measurements, J. Photochem. Photobiol. A Chem. 115 (1998) 89–97, https://doi.org/10.1016/S1010-6030(98)00264-0.

[7] V.L. Pugachev, A.K. Chibisov, Measurement of the quantum yield for intersystem crossing to the triplet state from flash response curves, J. Appl. Spectrosc. 23 (1975) 1481–1483, https://doi.org/10.1007/BF00615860.

[8] N.M. Barbosa Neto, L. De Boni, C.R. Mendonça, L. Misoguti, S.L. Queiroz, L. R. Dinelli, A.A. Batista, S.C. Zilio, Nonlinear absorption dynamics in Tetrapyridyl Metalloporphyrins, J. Phys. Chem. B 109 (2005) 17340–17345, https://doi.org/10.1021/jp052168i.

[9] F. Gotardo, L.H.Z. Cocca, T.V. Acunha, A. Longoni, J. Toldo, P.F.B. Gonçalves, B. A. Iglesias, L. De Boni, Investigating the intersystem crossing rate and triplet quantum yield of Protoporphyrin IX by means of pulse train fluorescence technique, Chem. Phys. Lett. 674 (2017) 48–57, https://doi.org/10.1016/j.cplett.2017.02.055.

[10] L.H.Z. Cocca, F. Gotardo, L.F. Sciuti, T.V. Acunha, B.A. Iglesias, L. de Boni, Investigation of excited singlet state absorption and intersystem crossing mechanism of isomeric *meso*-tetra(pyridyl)porphyrins containing peripheral polypyridyl platinum(II) complexes, Chem. Phys. Lett. 708 (2018) 1–10, https://doi.org/10.1016/j.cplett.2018.07.061.

[11] G. Donnert, C. Eggeling, S.W. Hell, Triplet-relaxation microscopy with bunched pulsed excitation, Photochem. Photobiol. Sci. 8 (2009) 481–485, https://doi.org/10.1039/B903357M.
[12] J. Mücksch, T. Spielmann, E. Sisamakis, J. Widengren, Transient state imaging of live cells using single plane illumination and arbitrary duty cycle excitation pulse trains: TRAST imaging of live cells by SPIM, J. Biophotonics 8 (2015) 392–400, https://doi.org/10.1002/jbio.201400015.
[13] K. Koynov, H.-J. Butt, Fluorescence correlation spectroscopy in colloid and interface science, Curr. Opin. Colloid Interface Sci. 17 (2012) 377–387, https://doi.org/10.1016/j.cocis.2012.09.003.
[14] A. Schönle, C. Von Middendorff, C. Ringemann, S.W. Hell, C. Eggeling, Monitoring triplet state dynamics with fluorescence correlation spectroscopy: Bias and correction, Microsc. Res. Tech. 77 (2014) 528–536, https://doi.org/10.1002/jemt.22368.
[15] N.M.M. Moura, C.I.V. Ramos, I. Linhares, S.M. Santos, M.A.F. Faustino, A. Almeida, J.A.S. Cavaleiro, F.M.L. Amado, C. Lodeiro, M.G.P.M.S. Neves, Synthesis, characterization and biological evaluation of cationic porphyrin–terpyridine derivatives, RSC Adv. 6 (2016) 110674–110685, https://doi.org/10.1039/C6RA25373C.
[16] H. Abrahamse, M.R. Hamblin, New photosensitizers for photodynamic therapy, Biochem. J. 473 (2016) 347–364, https://doi.org/10.1042/BJ20150942.
[17] H.-G. Jeong, M.-S. Choi, Design and properties of porphyrin-based singlet oxygen generator, Isr. J. Chem. 56 (2016) 110–118, https://doi.org/10.1002/ijch.201500026.
[18] A. Ormond, H. Freeman, Dye sensitizers for photodynamic therapy, Materials 6 (2013) 817–840, https://doi.org/10.3390/ma6030817.
[19] L.H.Z. Cocca, T.M.A. Oliveira, F. Gotardo, A.V. Teles, R. Menegatti, J.P. Siqueira, C. R. Mendonça, L.A.M. Bataus, A.O. Ribeiro, T.F.M. Souza, G.R.L. Souza, P. J. Gonçalves, L. De Boni, Tetracarboxy-phthalocyanines: from excited state dynamics to photodynamic inactivation against bovine herpesvirus type 1, J. Photochem. Photobiol. B Biol. 175 (2017) 1–8, https://doi.org/10.1016/j.jphotobiol.2017.08.019.
[20] E. Alves, M.A.F. Faustino, M.G.P.M.S. Neves, Â. Cunha, H. Nadais, A. Almeida, Potential applications of porphyrins in photodynamic inactivation beyond the medical scope, J. Photochem. Photobiol. C Photchem. Rev. 22 (2015) 34–57, https://doi.org/10.1016/j.jphotochemrev.2014.09.003.
[21] D.M.A. Vera, M.H. Haynes, A.R. Ball, T. Dai, C. Astrakas, M.J. Kelso, M.R. Hamblin, G.P. Tegos, Strategies to potentiate antimicrobial Photoinactivation by overcoming resistant phenotypes†, Photochem. Photobiol. 88 (2012) 499–511, https://doi.org/10.1111/j.1751-1097.2012.01087.x.
[22] M.P. Cormick, M.G. Alvarez, M. Rovera, E.N. Durantini, Photodynamic inactivation of Candida albicans sensitized by tri- and tetra-cationic porphyrin derivatives, Eur. J. Med. Chem. 44 (2009) 1592–1599, https://doi.org/10.1016/j.ejmech.2008.07.026.
[23] L. Costa, M.A.F. Faustino, J.P.C. Tomé, M.G.P.M.S. Neves, A.C. Tomé, J.A. S. Cavaleiro, Â. Cunha, A. Almeida, Involvement of type I and type II mechanisms on the photoinactivation of non-enveloped DNA and RNA bacteriophages, J. Photochem. Photobiol. B Biol. 120 (2013) 10–16, https://doi.org/10.1016/j.jphotobiol.2013.01.005.
[24] E. Alves, J.M.M. Rodrigues, M.A.F. Faustino, M.G.P.M.S. Neves, J.A.S. Cavaleiro, Z. Lin, Â. Cunha, M.H. Nadais, J.P.C. Tomé, A. Almeida, A new insight on nanomagnet–porphyrin hybrids for photodynamic inactivation of microorganisms, Dyes Pigments 110 (2014) 80–88, https://doi.org/10.1016/j.dyepig.2014.05.016.
[25] L. Lucantoni, M. Magaraggia, G. Lupidi, R.K. Ouedraogo, O. Coppellotti, F. Esposito, C. Fabris, G. Jori, A. Habluetzel, Novel, Meso-substituted cationic porphyrin molecule for photo-mediated larval control of the dengue vector Aedes aegypti, PLoS Negl. Trop. Dis. 5 (2011) e1434, https://doi.org/10.1371/journal.pntd.0001434.
[26] N.M.M. Moura, M.A.F. Faustino, M.G.P.M.S. Neves, F.A.A. Paz, A.M.S. Silva, A. C. Tomé, J.A.S. Cavaleiro, A new synthetic approach to benzoporphyrins and Kröhnke type porphyrin-2-ylpyridines, Chem. Commun. 48 (2012) 6142–6144, https://doi.org/10.1039/C2CC30727H.
[27] A.M. Brouwer, Standards for photoluminescence quantum yield measurements in solution (IUPAC technical report), Pure Appl. Chem. 83 (2011) 2213–2228, https://doi.org/10.1351/PAC-REP-10-09-31.
[28] L. De Boni, C. Toro, F.E. Hernandez, Excited state absorption study in Hematoporphyrin IX, J. Fluoresc. 20 (2010) 197–202, https://doi.org/10.1007/s10895-009-0538-z.
[29] P.J. Gonçalves, L.F. Sciuti, N.M.B. Neto, R.C. e Silva, E. Silveira-Alves, C. R. Mendonça, S.C. Zílio, I.E. Borissevitch, L. de Boni, Effects of pH on the ultrafast transient absorption of iron (III) meso-tetrakis(4-N-methyl-pyridiniumyl) porphyrin (Fe3+TMPyP) molecular complexes, J. Photochem. Photobiol. A Chem. 408 (2021) 113082, https://doi.org/10.1016/j.jphotochem.2020.113082.
[30] L.F. Sciuti, L.H.Z. Cocca, A.R.L. Caires, P.J. Gonçalves, L. de Boni, Picosecond dynamic of aqueous sodium-copper chlorophyllin solution: an excited state absorption study, Chem. Phys. Lett. 706 (2018) 652–657, https://doi.org/10.1016/j.cplett.2018.07.016.
[31] L.A. Padilha, S. Webster, O.V. Przhonska, H. Hu, D. Peceli, J.L. Rosch, M.V. Bondar, A.O. Gerasov, Y.P. Kovtun, M.P. Shandura, A.D. Kachkovski, D.J. Hagan, E.W. V. Stryland, Nonlinear absorption in a series of donor–π–acceptor cyanines with different conjugation lengths, J. Mater. Chem. 19 (2009) 7503–7513, https://doi.org/10.1039/B907344B.
[32] L.H.Z. Cocca, M.M. Ayhan, A.G. Gürek, V. Ahsen, Y. Bretonnière, J.D.P. Siqueira, F. Gotardo, C.R. Mendonça, C. Hirel, L.D. Boni, Mechanism of the Zn(II) phthalocyanines' photochemical reactions depending on the number of substituents and geometry, Molecules 21 (2016), https://doi.org/10.3390/molecules21050635.
[33] L. De Boni, L. Gaffo, L. Misoguti, C.R. Mendonça, Nonlinear absorption spectrum of ytterbium bis-phthalocyanine solution measured by white-light continuum Z-scan technique, Chem. Phys. Lett. 419 (2006) 417–420, https://doi.org/10.1016/j.cplett.2005.12.001.
[34] J. Kuśba, V. Bogdanov, I. Gryczynski, J.R. Lakowicz, Theory of light quenching: effects of fluorescence polarization, intensity, and anisotropy decays, Biophys. J. 67 (1994) 2024–2040, https://doi.org/10.1016/S0006-3495(94)80686-1.
[35] P. Hammond, Comparison of experimental and theoretical excited-state spectra for rhodamine 6G, IEEE J. Quantum Electron. 16 (1980) 1157–1160, https://doi.org/10.1109/JQE.1980.1070393.
[36] V.E. Korobov, V. Shubin, A. Chibisov, Triplet state of rhodamine dyes and its role in production of intermediates, Chem. Phys. Lett. 45 (1977) 498–501, https://doi.org/10.1016/0009-2614(77)80074-2.
[37] A. Ansari, A. Szabo, Theory of photoselection by intense light pulses. Influence of reorientational dynamics and chemical kinetics on absorbance measurements, Biophys. J. 64 (1993) 838–851, https://doi.org/10.1016/S0006-3495(93)81445-0.